

Development of Nano-Sulfide Sorbent for Efficient Removal of Elemental Mercury from Coal Combustion Fuel Gas

Hailong Li,^{†,§} Lei Zhu,[†] Jun Wang,[‡] Liqing Li,[†] and Kaimin Shih^{*,§}

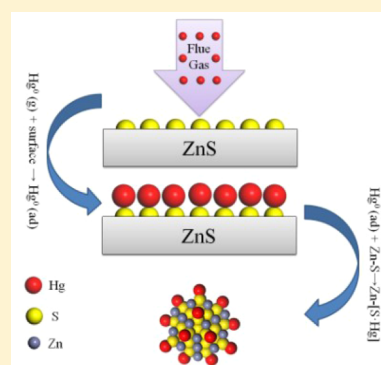
[†]School of Energy Science and Engineering, Central South University, Changsha, China 410083

[‡]Department of Occupational and Environmental Health, College of Public Health, University of Oklahoma Health Sciences Center, Oklahoma City, Oklahoma 73126, United States

[§]Department of Civil Engineering, The University of Hong Kong, Hong Kong SAR, China

Supporting Information

ABSTRACT: The surface area of zinc sulfide (ZnS) was successfully enlarged using nanostructure particles synthesized by a liquid-phase precipitation method. The ZnS with the highest surface area (named Nano-ZnS) of $196.1 \text{ m}^2 \cdot \text{g}^{-1}$ was then used to remove gas-phase elemental mercury (Hg^0) from simulated coal combustion fuel gas at relatively high temperatures (140 to 260 °C). The Nano-ZnS exhibited far greater Hg^0 adsorption capacity than the conventional bulk ZnS sorbent due to the abundance of surface sulfur sites, which have a high binding affinity for Hg^0 . Hg^0 was first physically adsorbed on the sorbent surface and then reacted with the adjacent surface sulfur to form the most stable mercury compound, HgS , which was confirmed by X-ray photoelectron spectroscopy analysis and a temperature-programmed desorption test. At the optimal temperature of 180 °C, the equilibrium Hg^0 adsorption capacity of the Nano-ZnS (inlet Hg^0 concentration of $65.0 \mu\text{g} \cdot \text{m}^{-3}$) was greater than $497.84 \mu\text{g} \cdot \text{g}^{-1}$. Compared with several commercial activated carbons used exclusively for gas-phase mercury removal, the Nano-ZnS was superior in both Hg^0 adsorption capacity and adsorption rate. With this excellent Hg^0 removal performance, noncarbon Nano-ZnS may prove to be an advantageous alternative to activated carbon for Hg^0 removal in power plants equipped with particulate matter control devices, while also offering a means of reusing fly ash as a valuable resource, for example as a concrete additive.



INTRODUCTION

The constantly updated air pollutants emission inventory confirms that coal combustion continues to be a major source of emissions, responsible for about 475 tons of mercury emissions annually.¹ Because of the extreme toxicity and bioaccumulation of methyl mercury transformed from emitted mercury,² China and the United States adopted national mercury standards to limit mercury emissions from coal-fired power plants by December 2011.^{3,4} Elemental mercury (Hg^0) is highly volatile and has a long lifespan in the atmosphere, thus making it a global environmental pollutant. As of March 2016, 128 nations have signed the Minamata Convention on Mercury to protect human health and the environment from the adverse effects of mercury from anthropogenic sources such as coal combustion. Various technologies, including activated carbon (AC) injection, have been developed to control mercury emissions from coal combustion to meet the requirements of global and regional mercury regulations.

Activated carbon injection is the maximum achievable control technology for mercury capture from coal-fired power plants.² Due to the limited mercury capture capacity of raw activated carbons,⁵ chemical emendations including sulfur,⁶ chlorine,⁷ and bromine⁸ impregnation are currently being developed to enhance the mercury adsorption capacities of the activated carbons that are injected upstream of particulate

matter control devices, which are either electrostatic precipitators or fabric filters. For example, sulfur-impregnated carbons perform much better than untreated carbon for gas-phase mercury removal.⁹ Under optimal conditions, removal rates greater than 90% can be attained with injections of these chemically impregnated activated carbons.⁸ However, the rates drop significantly depending on the coal quality and flue gas temperature,^{2,10} and production of the impregnated activated carbons requires toxic raw materials such as H_2S gas.¹¹ More importantly, injection of the impregnated activated carbons increases the carbon content of fly ash, thus preventing its reuse as a raw material for concrete.¹² Most coal fly ash wastes are dumped in landfills rather than being reused for beneficial purposes,¹³ and evaluations of the stability of mercury in the landfill or aqueous environment have shown that carbon materials facilitate mercury methylation.^{14,15} Many noncarbon sorbents can overcome most of the disadvantages associated with activated carbons and have thus been considered as alternatives.^{16–19} With chemical functionalization by sulfur, these noncarbon sorbents exhibit an excellent capacity for

Received: April 29, 2016

Revised: July 14, 2016

Accepted: August 10, 2016

Published: August 10, 2016

mercury removal,^{16,20,21} because mercury has a high binding affinity for reduced sulfur compounds such as sulfide (HS^- , S^{2-}). After adsorption, mercury forms extremely stable mercuric sulfide (HgS) species on the sorbent surface, and sorption capacities have been observed to correspond to a 1:1 molar ratio of Hg^0 : S .²⁰ Accordingly, adequate surface coverage of sulfur is critical to the Hg^0 adsorption performance of sulfur-containing noncarbon sorbents.²²

Mineral sulfides composed entirely of “active” sulfur sites are promising because they avoid the problem of surface sulfur coverage. Compared with the sulfurization of sorbents, the fabrication of sulfide-based sorbents is much simpler, more environmentally benign, and can even be achieved by reprocessing of mining wastes or ore materials containing mineral sulfides.²³ Moreover, mineral sulfides such as ZnS and FeS_2 are known to be stable²⁴ and have the ability to inhibit mercury methylation.²⁵ The low content of mineral sulfides in concrete is appealing, for example, ZnS in concrete not only exhibits no adverse effect on the concrete’s performance but also controls the release of heavy metals.²⁶ Taking these advantages into account, the use of mineral sulfides for removing mercury from coal combustion flue gas may be a scientifically sound and economically feasible strategy. However, only limited studies have investigated the removal of gas-phase mercury using mineral sulfides.^{27–29} A common issue with these studies is that they used mineral sulfides with small surface areas. Hence, their mercury adsorption capacities were found to be similar to or less than those of activated carbons.²⁷ However, when the mercury adsorption capacities are normalized to the surface area values, the mercury adsorption capacities of these mineral sulfides appear to be 100 times greater than those of activated carbons per unit surface area. Despite the flaws of these preliminary studies, these works provide strong hints that mineral sulfides with a larger surface area could be promising alternatives to activated carbon for gas-phase mercury removal.

The present study was based on the above hypothesis. The goal was to use nanostructures to develop a mineral sulfide with a large surface area for removing mercury from coal combustion flue gas. Nano-sphalerite (ZnS) was synthesized using a liquid-phase precipitation method to enlarge its surface area. Hg^0 removal performance was systematically evaluated under different gas atmospheres. The Hg^0 removal performance of Nano- ZnS and commercial activated carbons was compared. The mechanism responsible for the excellent Hg^0 removal performance of Nano- ZnS was also investigated.

■ EXPERIMENTAL SECTION

Adsorbent Preparation. ZnS samples were synthesized using a liquid-phase precipitation method. In a typical procedure, 1 M aqueous solution of zinc sulfate (ZnSO_4 , heptahydrate, 99.5 wt %, Sinopharm) and 1 M aqueous solution of ammonium sulfide ($(\text{NH}_4)_2\text{S}$, 20 wt %, Sinopharm) were prepared using double-distilled water. To adjust the surface areas of the final powder sorbents, trace amounts of hexadecyl trimethylammonium bromide (CTMAB; analytical grade, 99.0 wt %, Sinopharm) were added to the zinc sulfate solution while stirring. This was followed by the dropwise addition of an appropriate amount of 1 M ammonium sulfide solution under vigorous stirring to maintain the stoichiometric Zn/S ratio of 1:0.98. The resulting turbid dispersion was aged for different periods (0.5 to 2 h). The solution-containing products were then centrifuged, had the supernatant layer

poored off, and were washed 10 times with double-distilled water and 3 times with anhydrous ethanol (analytical grade, Sinopharm). The precipitates were dried in an oven at an elevated temperature for 12 h to obtain white samples, which were further grinded and sieved through 60/80 meshes (250/180 μm) before used in mercury removal experiments. By adjusting the preparation conditions, such as the amount of CTMAB and the aging time, three ZnS samples with different specific surface areas were obtained. The ZnS with the largest surface area was named Nano- ZnS in the present study.

A commercial ZnS reagent (analytical grade, 99.9 wt %, Aladdin) and two commercial activated carbons (BPL, Calgon Carbon Corporation, and TX, Tangxin Activated Carbon Corporation) exclusively used for mercury removal were used as comparison materials.

Powder Characterization. The Brunauer–Emmett–Teller (BET) specific surface area (S_{BET}) measurement by N_2 adsorption/desorption at -196°C was determined using a BET analyzer (ASAP-2020, Micromeritics). All samples were oven-dried at 110°C for 24 h and were degassed for 12 h at 180°C under vacuum conditions before the BET measurements. The crystal structures of the Nano- ZnS were determined using an X-ray diffractometer (XRD, SIMENS D500 Bruker) operating at 40 kV and 40 mA using $\text{Cu K}\alpha$ radiation ($\lambda = 0.15406\text{ nm}$) in the range of $10\text{--}80^\circ$ (2θ) with a step size of $0.02^\circ/\text{s}$. The patterns recorded were compared with the powder diffraction files in the PDF-2 database for identification of the crystal phases. A 200 kV transmission electron microscopy (TEM) setup (Tecnai G2 F20 FEI) with a resolution of 0.2 nm was used for microstructure imaging and determination of the Nano- ZnS .

Identification of Mercury Species on Nano- ZnS after Adsorption. X-ray photoelectron spectroscopy (XPS) analysis for identifying mercury species on the sorbent surface was conducted on an XPS (Escalab 250Xi, Thermo Fisher Scientific), with a monochromatized $\text{Al K}\alpha$ radiation ($h\nu = 1486.6\text{ eV}$) as the excitation source. The oven-dried sample was degassed in a vacuum oven for 12 h before the XPS analysis. The vacuum of the XPS equipment was maintained at 10^{-6} Pa . Sample charging effects were eliminated by correcting the observed spectra with the C 1s binding energy (BE) value of 284.6 eV. Mercury species on the Nano- ZnS were identified through a novel temperature-programmed desorption (TPD) method. In the TPD experiments, Hg^0 from the decomposition of mercury compounds on the Nano- ZnS sorbent was extracted from the reactor using a gas stream of pure nitrogen at a flow rate of $250\text{ mL}\cdot\text{min}^{-1}$. The heating rate from room temperature to 600°C was nominally $5^\circ\text{C}\cdot\text{min}^{-1}$. HgS diluted with fresh Nano- ZnS was first tested in the TPD system to determine a specific profile that served as a standard for identifying mercury species on the Nano- ZnS after the adsorption of Hg^0 .

Experimental Setup and Method. The Hg^0 adsorption performances of ZnS adsorbents were evaluated using the bench-scale experimental system shown in Figure S1. All individual flue gas components were from cylinder gases and were precisely controlled by mass flow controllers, with a total flow rate of $1\text{ L}\cdot\text{min}^{-1}$. An N_2 flow ($200\text{ mL}\cdot\text{min}^{-1}$), serving as a carrier gas, passed through an Hg^0 permeation device (VICI Metronics) loaded in a U-shaped glass tube to obtain Hg^0 for the simulated coal combustion flue gas. The U-shaped glass tube was placed in a temperature-controlled water bath to maintain the Hg^0 concentration at $65.0 \pm 1.0\ \mu\text{g}\cdot\text{m}^{-3}$. A borosilicate glass reactor, with an inner diameter of 10 mm and

a length of 650 mm, was put in a temperature-controlled tubular furnace to maintain the reaction temperature with fluctuations of less than 1.0 °C. 200 ± 5 mg of sorbent was placed in the reaction zone of the reactor during each experiment. All tubes and valves that were in contact with Hg⁰ were constructed from Teflon, which has been demonstrated to be chemically inert toward Hg⁰. The Hg⁰ concentrations at both the inlet and outlet of the reactor were monitored online by a mercury analyzer (VM3000, Mercury Instruments, Inc.) based on cold vapor absorption spectrometry. The exhaust gas was treated by an activated carbon trap before discharge.

Four sets of experiments were conducted. The details are summarized in Table S1. The experiments in Set I were carried out to study the effect of specific surface area on Hg⁰ adsorption over ZnS. The experiments in Set II were designed to evaluate the Hg⁰ removal performance of Nano-ZnS at 140–260 °C under pure N₂, N₂ plus 4% O₂, and simulated coal combustion flue gas (SFG, 4% O₂, 8% H₂O, 10 ppm of HCl, 300 ppm of NO, 400 ppm of SO₂), respectively. The experiments in Set III were conducted to determine the Hg⁰ adsorption capacities of Nano-ZnS. Direct comparisons of the Hg⁰ adsorption performances of Nano-ZnS and commercial ACs under an N₂ atmosphere were conducted in the Set IV experiments.

At the beginning of each test, the gas stream bypassed the reactor and the inlet gas was monitored until the desired inlet Hg⁰ concentration (C_{in}) had been stabilized for at least 30 min. The gas flow was then passed through the reactor and taken from the exit of the reactor to measure the outlet Hg⁰ concentration (C_{out}). The Hg⁰ absorption capacity of a known weight of sorbent for the online Hg⁰ analyzer tests was calculated in terms of micrograms (μg) of Hg⁰ adsorbed per gram (g) of sorbent from the breakthrough curve (outlet Hg⁰ concentration versus time). The area under the inlet Hg⁰ concentration line and above a breakthrough curve was used to determine the quantity of Hg⁰ adsorbed by the sorbent. Therefore, Hg⁰ absorption capacity values were obtained according to eq 1

$$Q = \frac{1}{m} \int_{t_1}^{t_2} (C_{in} - C_{out}) \times f \times dt \quad (1)$$

where Q is the Hg⁰ absorption capacity (μg·g⁻¹), f is the gas flow rate (m³·h⁻¹), m is the mass of sorbent (g), and t is the adsorption time (h). For each experiment, two replicates were conducted, and the mean value was reported. For most experiments, the relative errors were less than 5%.

RESULTS AND DISCUSSION

Characterization of Sorbents. The BET specific surface area of the ZnS agent was 28.3 m²·g⁻¹. The prepared ZnS samples exhibited different specific surface areas of 64.6 m²·g⁻¹, 105.9 m²·g⁻¹, and 196.1 m²·g⁻¹, respectively. This indicates that the specific surface area of ZnS can be easily controlled by adjusting the preparation conditions during the liquid-phase precipitation processes. The XRD pattern of the Nano-ZnS with the largest surface area of 196.1 m²·g⁻¹ is shown in Figure S2. Various diffraction peaks at different 2θ values correspond to the (111), (220), and (311) diffraction planes, respectively. The peaks were perfectly indexed to the cubic zinc blende phase of ZnS. As broad diffraction peaks on the XRD pattern can be attributed to characteristic small particle effects,³⁰ the

typical broadening of the three diffraction peaks on the XRD pattern of the Nano-ZnS implies that the size of the ZnS crystals was in the nanometer range. The mean diameter of the ZnS nanocrystals was calculated using the Debye–Scherrer Equation³¹ with (111) reflection in the XRD pattern. The results show that the mean diameter of the ZnS nanocrystal was about 6 nm, which is close to the 4.5 nm measurement obtained from the TEM image shown in Figure S3. Figure S3 also shows that the ZnS nanocrystals were highly dispersed.

ZnS with Different Surface Areas for Gas-Phase Hg⁰ Removal. The commercial ZnS agent and synthesized ZnS samples with different specific surface areas were adopted to remove Hg⁰ from the N₂ gas flow at 140 °C. As shown in Figure 1, the normalized outlet Hg⁰ concentration (to inlet

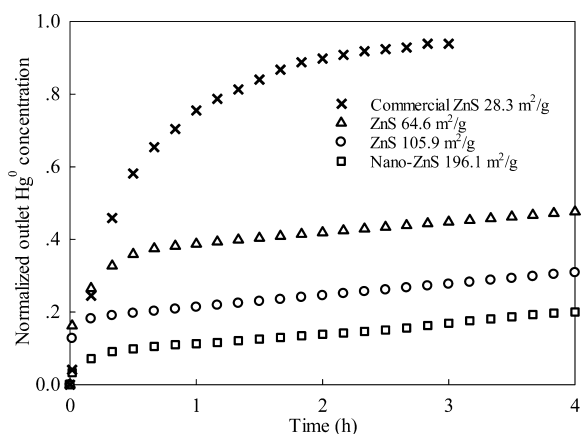


Figure 1. Hg⁰ removal over ZnS samples with different surface areas.

concentration) quickly climbed to 0.80 after gas flow passed through the commercial ZnS agent. The commercial ZnS agent exhibited an insignificant absorption capacity for gas-phase Hg⁰. This finding is consistent with a previous study in which mineral sulfides with a small surface area exhibited a weak capacity for removing Hg⁰ from flue gas.²⁷ Better Hg⁰ removal performance was observed on the synthesized ZnS samples with larger surface areas. No synthesized ZnS sample had a breakthrough at the end of the 4-h experiment. Lower outlet Hg⁰ concentrations were observed on the ZnS sorbents with larger surface areas. This result is similar to findings from an earlier study where ground and kneaded FeS₂ ore with greater porosity was more effective for Hg⁰ removal than the original FeS₂ ore.²⁸ This phenomenon also indicates that the specific surface area plays an important role in Hg⁰ capture, and a large surface area facilitates Hg⁰ adsorption over ZnS. For the Nano-ZnS with the largest surface area, the normalized outlet Hg⁰ concentration was less than 0.20 during the entire experimental period, indicating that Nano-ZnS is effective for gas-phase Hg⁰ removal. This provided preliminary confirmation of our hypothesis. The subsequent section of this study focuses on the Nano-ZnS, as it exhibited the best performance for gas-phase Hg⁰ removal.

Performance of Nano-ZnS for Removal of Hg⁰ from Flue Gas. The Hg⁰ removal performance of the optimal Nano-ZnS was evaluated from 140 to 260 °C under different flue gas atmospheres: pure N₂, N₂ plus 4% O₂, and SFG. The results are shown in Figures 2(a), 2(b), and 2(c), for the pure N₂, N₂ plus 4% O₂, and SFG scenarios, respectively.

As shown in Figure 2(a), the normalized outlet Hg⁰ concentrations gradually increased from 0.04 to 0.20 during a

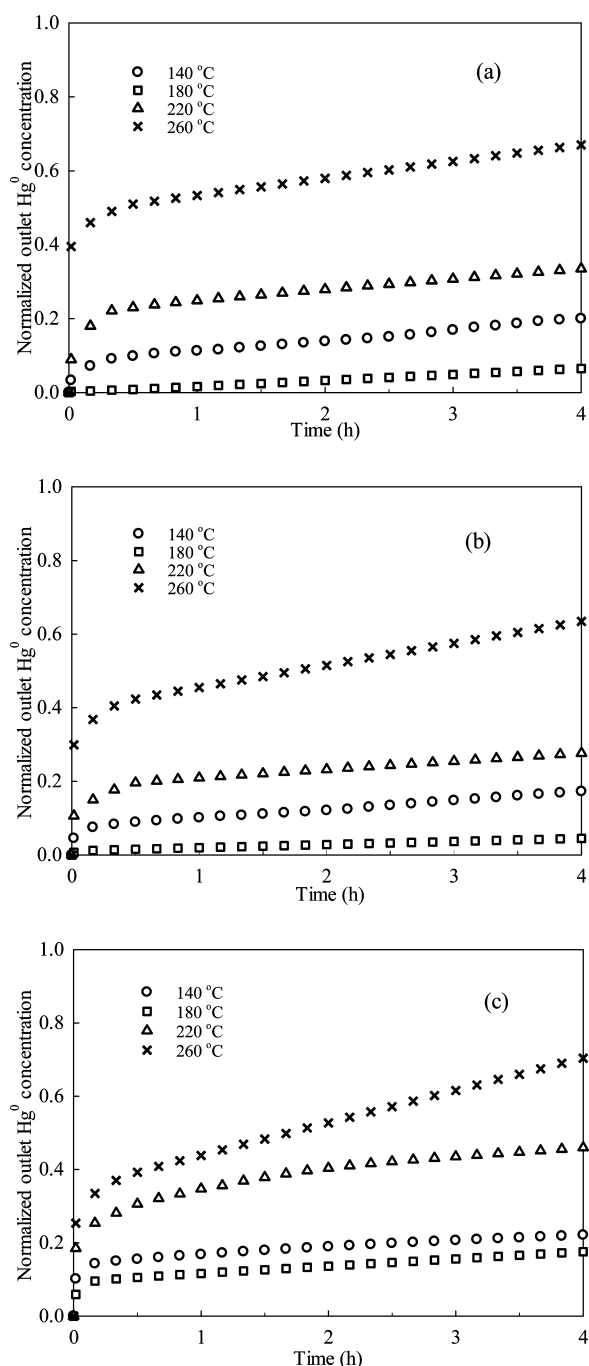


Figure 2. Breakthrough curves for Nano-ZnS under different flue gas conditions (a: N_2 ; b: $N_2 + 4\% O_2$; c: SFG).

4-h test at 140 °C. More Hg^0 was adsorbed when the temperature increased to 180 °C. At the end of the 4-h test, the normalized outlet Hg^0 concentration was less than 0.10. The capacity of Hg^0 adsorption onto Nano-ZnS increased as the adsorption temperature increased, suggesting a chemical adsorption mechanism. However, further increases in temperature to 220 and 260 °C reduced the Hg^0 removal performance of the Nano-ZnS. At 260 °C, the normalized outlet Hg^0 concentration instantaneously climbed to 0.40 after the N_2 gas flow containing Hg^0 passed through the Nano-ZnS sorbent, indicating that the high temperature inhibited Hg^0 adsorption and/or facilitated the decomposition of mercury compounds. Nano-ZnS exhibited the best Hg^0 adsorption performance at

180 °C. This is in line with a previous study, in which the optimal gas-phase Hg^0 removal temperature for bulk ZnS was found to be around 180 °C.²⁹ The optimal operating temperatures for Nano-ZnS and bulk ZnS were close to each other, indicating similar Hg^0 adsorption mechanisms for both types of ZnS.

The profiles of the normalized outlet Hg^0 concentration as a function of time for Nano-ZnS under N_2 plus 4% O_2 atmosphere are shown in Figure 2(b). Almost the same trend was observed as that in the pure N_2 scenario. At the end of the 4-h test, the normalized outlet Hg^0 concentration decreased from 0.17 to 0.05 as the temperature rose from 140 to 180 °C and then ascended sharply from 0.05 to 0.63 when the temperature further rose to 260 °C. The optimal temperature for Hg^0 removal in the presence of O_2 was observed to be 180 °C. Compared with Hg^0 adsorption without O_2 , the presence of O_2 had a slight promotional effect on Hg^0 adsorption over Nano-ZnS at 140 and 180 °C. However, this promotional effect became more obvious as the temperature increased. This indicates that O_2 facilitates Hg^0 chemisorption, which generally takes place at high flue gas temperatures.

To further identify the Hg^0 removal performance of Nano-ZnS, Hg^0 adsorption experiments were conducted under simulated coal combustion flue gas. As shown in Figure 2(c), Nano-ZnS exhibited excellent performance for adsorption of Hg^0 from simulated coal combustion flue gas at temperatures below 180 °C. After a 4-h test, the normalized outlet Hg^0 concentrations at 140 and 180 °C were less than 0.25. It should be noted that the inlet Hg^0 concentration was much higher than that of the real coal combustion flue gas, and the corresponding gas hourly space velocity (GHSV) was very high.³² Therefore, we can conclude that Nano-ZnS with a large surface area is efficient for the removal of gas-phase Hg^0 from coal combustion flue gas, further confirming our hypothesis. Moreover, the efficiency-to-temperature trend in this simulated coal combustion flue gas scenario was similar to that observed in the pure N_2 and N_2 plus O_2 scenarios. This indicates that most of the flue gas components had an insignificant effect on Hg^0 adsorption over Nano-ZnS, which is a huge advantage for removing Hg^0 from coal combustion flue gas.¹⁰ With this advantage, the application of Nano-ZnS is likely to be beneficial to Hg^0 removal from coal-fired power plants burning high-sulfur coals.

Comparison of the Hg^0 Adsorption Capacities of Nano-ZnS and Commercial ACs. In the set III experiments, a relatively long test was conducted under N_2 and N_2 plus 4% O_2 atmospheres at 180 °C with an inlet Hg^0 concentration of $65 \mu g \cdot m^{-3}$. Hg^0 adsorption capacities were obtained according to eq 1, using the breakthrough curves shown in Figure S4. When the normalized outlet Hg^0 concentration reached 50%, Hg^0 adsorption capacities of $472.1 \mu g \cdot g^{-1}$ and $497.8 \mu g \cdot g^{-1}$ were obtained in N_2 and N_2 plus 4% O_2 , respectively. It is reasonable to assume that the equilibrium Hg^0 adsorption capacity of Nano-ZnS could be much greater when the breakthrough point is reached, i.e., when the normalized outlet Hg^0 concentration is equal to 1.0. For comparison, the equilibrium adsorption capacities of different commercial ACs reported in the literature^{9,16,27,33–38} are presented in Table S2. As shown, Nano-ZnS exhibited a much greater Hg^0 adsorption capacity than all of the carbon materials listed as comparison materials, even though the flue gas temperature was relatively high and the inlet Hg^0 concentration was relatively low.

A direct comparison of Hg^0 adsorption performance was conducted on the same experimental system (shown in Figure S1) under the same experimental conditions, the results of which are presented in Figure 3. As shown, the Hg^0 adsorption

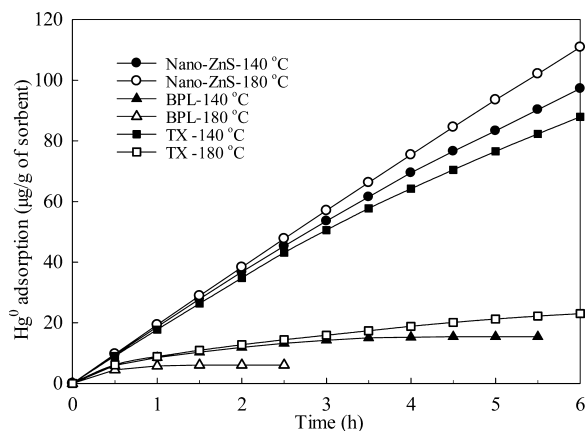


Figure 3. Comparison of Hg^0 adsorption capacities of Nano-ZnS and commercial ACs.

capacity of Nano-ZnS was much greater than that of BPL AC at 140 °C. At the end of the 6-h tests, 1 g of the Nano-ZnS adsorbed 98.6 μg Hg^0 , while the BPL AC only adsorbed 14.6 μg Hg^0 . The Hg^0 adsorption performance of TX AC was comparable to that of Nano-ZnS at 140 °C. However, when the temperature increased from 140 to 180 °C, the Hg^0 adsorption capacity of the TX AC dramatically reduced from 87.92 to 23.0 $\mu\text{g}\cdot\text{g}^{-1}$, which is much lower than the 110.9 $\mu\text{g}\cdot\text{g}^{-1}$ observed for the Nano-ZnS. This phenomenon has also been described in the literature,^{39,40} in which the mercury removal effectiveness of standard AC dropped rapidly when the temperature approached 180 °C. Moreover, the Hg^0 adsorption rate of Nano-ZnS, represented by the slope of the adsorption curve presented in Figure 3, was still high at the end of the 6-h test. In contrast, the Hg^0 adsorption rate of the TX AC began to decelerate, and that of the BPL AC was negligible. A higher Hg^0 adsorption rate of the Nano-ZnS would warrant less adsorbent consumption for the same Hg^0 removal efficiency request. Therefore, it is reasonable to conclude that Nano-ZnS with a large surface area is a superior and probably cost-effective noncarbon adsorbent for removal of mercury from coal combustion flue gas.

Mechanism Involved in Hg^0 Adsorption by Nano-ZnS.

Extensive studies have been conducted to understand the Hg^0 adsorption mechanisms of sulfur-impregnated activated carbon and inorganic substrates.^{20,34,38} However, few of these studies focused on Hg^0 removal over mineral sulfides, and they provided very little information about the detailed adsorption mechanisms. To explore the Hg^0 removal mechanisms on the Nano-ZnS sorbent, fresh Nano-ZnS was pretreated (saturated by Hg^0 at 180 °C under 300 $\mu\text{g}\cdot\text{m}^{-3}$ Hg^0 balanced in N_2 for several days and then purged with pure N_2 until Hg^0 discharged from the reactor outlet was below the detection limit) to obtain a pretreated, mercury-loaded Nano-ZnS. XPS analysis was conducted to identify the valence state of mercury on the pretreated Nano-ZnS, and the XPS spectrum of Hg 4f is presented in Figure 4 (a). As shown, the Hg 4f spectrum possessed an obvious peak at 100.8 eV, which confirms the transformation of Hg^0 to other mercury species on the Nano-ZnS surface because the peak for Hg 4f 7/2 associated with Hg^0

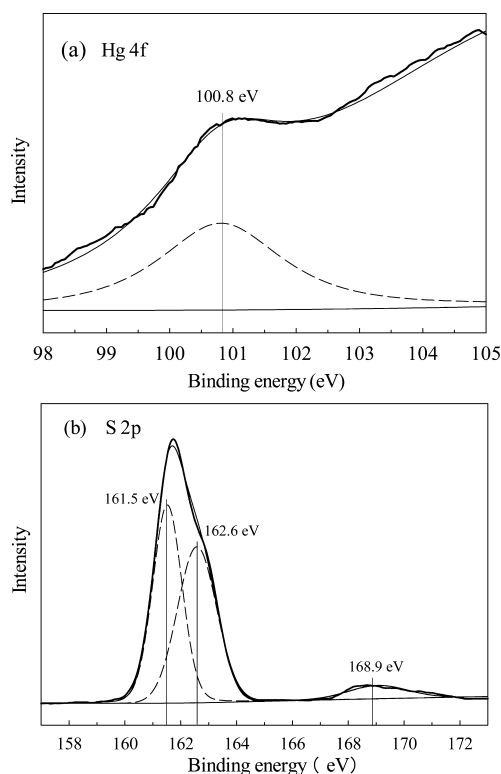


Figure 4. Hg 4f (a) and S 2p (b) XPS spectra of pretreated Nano-ZnS.

around 99.9 eV was not observed in the XPS spectrum.^{41,42} This further confirms that Hg^0 chemical adsorption occurred over the Nano-ZnS at 180 °C. Even if a small amount of Hg^0 was physically adsorbed on the Nano-ZnS surface, most would have been flushed away during the pretreatment and/or vacuumization of the XPS chamber. The peak at 100.8 eV could be ascribed to both HgO and HgS .²⁹ However, because the surface of the Nano-ZnS turned black after pretreatment, black HgS was considered the potential mercury species on the sorbent surface, rather than HgO . The XPS spectrum of the S 2p level for the Nano-ZnS is shown in Figure 4(b). The two peaks at lower binding energies of 161.5 and 162.6 eV were assigned to S^{2-} . This is in agreement with the difference in energy predicted by the spin-orbit splitting.⁴³ Another peak at 168.9 eV was ascribed to S^{6+} .⁴⁴ The S^{6+} content was negligible compared with S^{2-} . Therefore, the results of the XPS analysis suggested that HgS was the main mercury species after Hg^0 adsorption over the Nano-ZnS.

It is possible to identify the mercury species present in different solids using a temperature-programmed decomposition method.^{45,46} Mercury species can be identified from the high peak temperature at which they are released, by comparing their desorption profiles with the desorption profiles of the reference pure mercury compounds. Pure HgS diluted with fresh Nano-ZnS was first tested to determine its specific profile. This then served as a fingerprint for comparison with the profile obtained from the pretreated Nano-ZnS, because HgS was identified by XPS analysis as the potential product of Hg^0 adsorption on the Nano-ZnS. As shown in Figure 5, no Hg^0 peak was observed for the Nano-ZnS that was free of mercury. Decomposition of pure HgS occurred at temperatures ranging from 180 to 380 °C, with a peak at approximately 300 °C, which is close to that reported in the literature.⁴⁶ Mercury species on the pretreated Nano-ZnS decomposed from 180 to

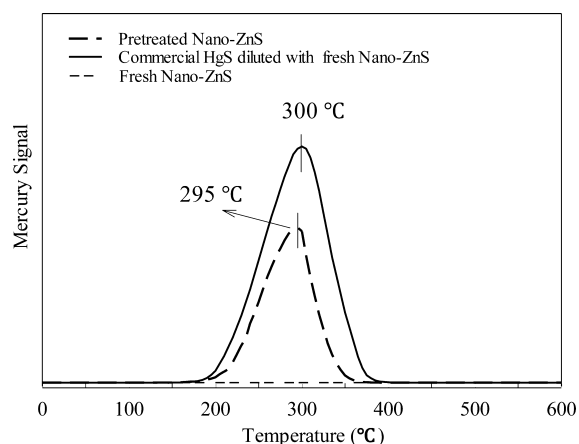
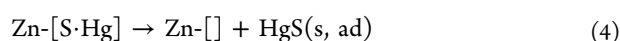
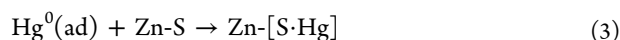
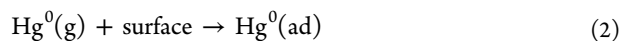


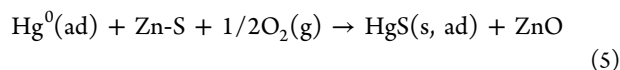
Figure 5. TPD spectrum of pretreated Nano-ZnS.

350 °C and presented a characteristic peak at 295 °C. These findings clearly demonstrate that the mercury species on the Nano-ZnS after Hg^0 adsorption presented mainly as HgS . The large surface area of the Nano-ZnS probably promoted the decomposition of HgS . Hence, the high peak temperature and complete decomposition temperature of the mercury-laden Nano-ZnS was slightly lower than that of the HgS agent physically diluted with Nano-ZnS.

As HgS was identified as the main mercury species on the Nano-ZnS after Hg^0 adsorption, a mechanism similar to that reported in the literature⁴⁷ may be responsible for Hg^0 adsorption over the Nano-ZnS adsorbent, the overall process of which is speculated to be



where $[\text{S·Hg}]$ represents the chemisorption compound, and $[]$ is the coordinative unsaturated site. Hg^0 in gas flow first made contact with and was physically adsorbed on the surface of the Nano-ZnS. The physically adsorbed Hg^0 then combined with sulfur atoms (S) that were well dispersed on the Nano-ZnS surface. Finally, Hg^0 was immobilized as stable HgS on the sorbent surface. With the aid of gas-phase O_2 , physically adsorbed Hg^0 could also react with adjacent ZnS, through the process in eq 5, to form HgS on the surface,⁴⁸ the Gibbs free energy change (ΔG) of which is far less than zero at flue gas temperatures. A negative ΔG indicates that the reaction through eq 5 could spontaneously take place on the surface of the Nano-ZnS. Higher temperatures accelerated reaction 5. Therefore, the gas-phase O_2 exhibited a more promotional effect on the transformation of Hg^0 to HgS at a higher temperature.



■ ASSOCIATED CONTENT

Supporting Information

The Supporting Information is available free of charge on the ACS Publications website at DOI: 10.1021/acs.est.6b02115.

Tables S1 and S2 and Figures S1–S4 (PDF)

■ AUTHOR INFORMATION

Corresponding Author

*Phone: 86-18670016725. Fax: 86-731-88879863. E-mail: kshih@hku.hk.

Notes

The authors declare no competing financial interest.

■ ACKNOWLEDGMENTS

This project was supported by the National Natural Science Foundation of China (no. 51476189), Hong Kong Scholar Program (no. XJ2014033), and General Research Fund (17206714, 17212015) of the Research Grants Council of Hong Kong.

■ REFERENCES

- (1) UNEP Global Mercury Assessment 2013: Sources, emissions, releases, and environmental transport, 2013. <http://www.unep.org> (accessed Jan 2015).
- (2) Pavlish, J. H.; Sondreal, E. A.; Mann, M. D.; Olson, E. S.; Galbreath, K. C.; Laudal, D. L.; Benson, S. A. Status review of mercury control options for coal-fired power plants. *Fuel Process. Technol.* **2003**, *82* (2–3), 89–165.
- (3) Ministry of Environmental Protection The People's Republic of China, Emission standard of air pollutants for thermal power plants (GB 13223-2011). <http://kjs.mep.gov.cn/hjbhbz/bzwb/dqjhbh/dqgdwrywrwpfbz/201109/W020130125407916122018.pdf> (accessed Jan 2015).
- (4) U.S. Environmental Protection Agency, Air Toxics Standards for Utilities. <http://www.epa.gov/ttn/atw/utility/utilitypg.html> (accessed July 2015).
- (5) Liu, Y.; Kelly, D. J. A.; Yang, H.; Lin, C. C. H.; Kuznicki, S. M.; Xu, Z. Novel regenerable sorbent for mercury capture from flue gases of coal-fired power plant. *Environ. Sci. Technol.* **2008**, *42* (16), 6205–6210.
- (6) Korpiel, J. A.; Vidic, R. D. Effect of sulfur impregnation method on activated carbon uptake of gas-phase mercury. *Environ. Sci. Technol.* **1997**, *31* (8), 2319–2325.
- (7) Lee, S. S.; Lee, J. Y.; Keener, T. C. Bench-scale studies of in-duct mercury capture using cupric chloride-impregnated carbons. *Environ. Sci. Technol.* **2009**, *43* (8), 2957–2962.
- (8) Jones, A. P.; Hoffmann, J. W.; Smith, D. N.; Feeley, T. J.; Murphy, J. T. DOE/NETL's Phase II mercury control technology field testing program: preliminary economic analysis of activated carbon injection. *Environ. Sci. Technol.* **2007**, *41* (4), 1365–1371.
- (9) Liu, W.; Vidić, R. D.; Brown, T. D. Optimization of sulfur impregnation protocol for fixed-bed application of activated carbon-based sorbents for gas-phase mercury removal. *Environ. Sci. Technol.* **1998**, *32* (4), 531–538.
- (10) Presto, A. A.; Granite, E. J. Impact of sulfur oxides on mercury capture by activated carbon. *Environ. Sci. Technol.* **2007**, *41* (18), 6579–6584.
- (11) Feng, W.; Borguet, E.; Vidic, R. D. Sulfurization of a carbon surface for vapor phase mercury removal - II: Sulfur forms and mercury uptake. *Carbon* **2006**, *44* (14), 2998–3004.
- (12) Ding, F.; Zhao, Y.; Mi, L.; Li, H.; Li, Y.; Zhang, J. Removal of gas-phase elemental mercury in flue gas by inorganic chemically promoted natural mineral sorbents. *Ind. Eng. Chem. Res.* **2012**, *51* (7), 3039–3047.
- (13) Ahmaruzzaman, M. A review on the utilization of fly ash. *Prog. Energy Combust. Sci.* **2010**, *36* (3), 327–363.
- (14) Ruhl, L.; Vengosh, A.; Dwyer, G. S.; Hsu-Kim, H.; Deonaraine, A.; Bergin, M.; Kravchenko, J. Survey of the potential environmental and health impacts in the immediate aftermath of the coal ash spill in Kingston, Tennessee. *Environ. Sci. Technol.* **2009**, *43* (16), 6326–6333.
- (15) Gilmour, C. C.; Henry, E. A.; Mitchell, R. Sulfate stimulation of mercury methylation in freshwater sediments. *Environ. Sci. Technol.* **1992**, *26* (11), 2281–2287.

- (16) Lee, J. Y.; Ju, Y. H.; Keener, T. C.; Varma, R. S. Development of cost-effective noncarbon sorbents for Hg⁰ removal from coal-fired power plants. *Environ. Sci. Technol.* **2006**, *40* (8), 2714–2720.
- (17) Yang, J.; Zhao, Y.; Zhang, J.; Zheng, C. Regenerable cobalt oxide loaded magnetosphere catalyst from fly ash for mercury removal in coal combustion flue gas. *Environ. Sci. Technol.* **2014**, *48*, 14837–14843.
- (18) Xie, J.; Xu, H.; Qu, Z.; Huang, W.; Chen, W.; Ma, Y.; Zhao, S.; Liu, P.; Yan, N. Sn-Mn binary metal oxides as non-carbon sorbent for mercury removal in a wide-temperature window. *J. Colloid Interface Sci.* **2014**, *428* (0), 121–127.
- (19) Zhang, L.; Zhuo, Y.; Du, W.; Tao, Y.; Chen, C.; Xu, X. Hg removal characteristics of noncarbon sorbents in a fixed-bed reactor. *Ind. Eng. Chem. Res.* **2012**, *51* (14), 5292–5298.
- (20) Otani, Y.; Kanaoka, C.; Emi, H.; Uchijima, I.; Nishino, H. Removal of mercury vapor from air with sulfur-impregnated adsorbents. *Environ. Sci. Technol.* **1988**, *22* (6), 708–711.
- (21) Makkuni, A.; Varma, R.; Sikdar, S.; Bhattacharyya, D. Vapor phase mercury sorption by organic sulfide modified bimetallic iron-copper nanoparticle aggregates. *Ind. Eng. Chem. Res.* **2007**, *46* (4), 1305–1315.
- (22) Wu, S.; Oya, N.; Ozaki, M.; Kawakami, J.; Uddin, M. A.; Sasaoka, E. Development of iron oxide sorbents for Hg⁰ removal from coal derived fuel gas: Sulfidation characteristics of iron oxide sorbents and activity for COS formation during Hg⁰ removal. *Fuel* **2007**, *86* (17–18), 2857–2863.
- (23) Martellaro, P.; Moore, G.; Peterson, E.; Abbott, E.; Gorenbain, A. Environmental application of mineral sulfides for removal of gas-phase Hg⁰ and aqueous Hg²⁺. *Sep. Sci. Technol.* **2001**, *36* (5–6), 1183–1196.
- (24) Lau, B. L.; Hsu-Kim, H. Precipitation and growth of zinc sulfide nanoparticles in the presence of thiol-containing natural organic ligands. *Environ. Sci. Technol.* **2008**, *42* (19), 7236–7241.
- (25) Benoit, J. M.; Gilmour, C. C.; Mason, R. P.; Heyes, A. Sulfide controls on mercury speciation and bioavailability to methylating bacteria in sediment pore waters. *Environ. Sci. Technol.* **1999**, *33* (10), 1780–1780.
- (26) Shi, H.-s.; Shi, H.-c. Study of effect of sulfide on zinc ion in cement-based materials. *Cement* **2006**, *02*, 15–18.
- (27) Granite, E. J.; Pennline, H. W.; Hargis, R. A. Novel sorbents for mercury removal from flue gas. *Ind. Eng. Chem. Res.* **2000**, *39* (4), 1020–1029.
- (28) Wu, S.; Ozaki, M.; Uddin, M. A.; Sasaoka, E. Development of iron-based sorbents for Hg⁰ removal from coal derived fuel gas: Effect of hydrogen chloride. *Fuel* **2008**, *87* (4–5), 467–474.
- (29) Takaoka, M.; Takeda, N.; Shimaoka, Y.; Fujiwara, T. Removal of mercury in flue gas by the reaction with sulfide compounds. *Toxicol. Environ. Chem.* **1999**, *73* (1–2), 1–16.
- (30) Qadri, S. B.; Skelton, E. F.; Hsu, D.; Dinsmore, A. D.; Yang, J.; Gray, H. F.; Ratna, B. R. Size-induced transition-temperature reduction in nanoparticles of ZnS. *Phys. Rev. B: Condens. Matter Mater. Phys.* **1999**, *60* (13), 9191–9193.
- (31) Suyver, J. F.; Wuister, S. F.; Kelly, J. J.; Meijerink, A. Synthesis and photoluminescence of nanocrystalline ZnS:Mn²⁺. *Nano Lett.* **2001**, *1* (8), 429–433.
- (32) Li, H.; Wu, C. Y.; Li, Y.; Zhang, J. CeO₂-TiO₂ catalysts for catalytic oxidation of elemental mercury in low-rank coal combustion flue gas. *Environ. Sci. Technol.* **2011**, *45*, 7394–7400.
- (33) Krishnan, S. V.; Gullett, B. K.; Jozewicz, W. Sorption of elemental mercury by activated carbons. *Environ. Sci. Technol.* **1994**, *28* (8), 1506–1512.
- (34) Vidic, R. D.; Chang, M. T.; Thurnau, R. C. Kinetics of vapor-phase mercury uptake by virgin and sulfur-impregnated activated carbons. *J. Air Waste Manage. Assoc.* **1998**, *48* (3), 247–255.
- (35) Liu, W.; Vidic, R. D.; Brown, T. D. Impact of flue gas conditions on mercury uptake by sulfur-impregnated activated carbon. *Environ. Sci. Technol.* **2000**, *34* (1), 154–159.
- (36) Hayashi, T.; Lee, T. G.; Hazelwood, M.; Hedrick, E.; Biswas, P. Characterization of activated carbon fiber filters for pressure drop, submicrometer particulate collection, and mercury capture. *J. Air Waste Manage. Assoc.* **2000**, *50* (6), 922–929.
- (37) De, M.; Azargohar, R.; Dalai, A. K.; Shewchuk, S. R. Mercury removal by bio-char based modified activated carbons. *Fuel* **2013**, *103*, 570–578.
- (38) Wei, Y.; Yu, D.; Tong, S.; Jia, C. Q. Effects of H₂SO₄ and O₂ on Hg⁰ uptake capacity and reversibility of sulfur-impregnated activated carbon under dynamic conditions. *Environ. Sci. Technol.* **2015**, *49* (3), 1706–1712.
- (39) Srivastava, R. K.; Hutson, N.; Martin, B.; Princiotta, F.; Staudt, J. Control of mercury emissions from coal-fired electric utility boilers. *Environ. Sci. Technol.* **2006**, *40* (5), 1385–1393.
- (40) Ochiai, R.; Uddin, M. A.; Sasaoka, E.; Wu, S. J. Effects of HCl and SO₂ concentration on mercury removal by activated carbon sorbents in coal-derived flue gas. *Energy Fuels* **2009**, *23*, 4734–4739.
- (41) Lee, W.; Bae, G. N. Removal of elemental mercury (Hg⁰) by nanosized V₂O₅/TiO₂ catalysts. *Environ. Sci. Technol.* **2009**, *43* (5), 1522–1527.
- (42) Hutson, N. D.; Attwood, B. C.; Scheckel, K. G. XAS and XPS characterization of mercury binding on brominated activated carbon. *Environ. Sci. Technol.* **2007**, *41* (5), 1747–1752.
- (43) Barreca, D.; Gasparotto, A.; Maragno, C.; Tondello, E.; Spalding, T. R. Analysis of nanocrystalline ZnS thin films by XPS. *Surf. Sci. Spectra* **2002**, *9* (1), 54–61.
- (44) Baláž, P.; Bastl, Z.; Briančin, J.; Ebert, I.; Lipka, J. Surface and bulk properties of mechanically activated zinc sulphide. *J. Mater. Sci.* **1992**, *27* (3), 653–657.
- (45) Lopez-Anton, M. A.; Perry, R.; Abad-Valle, P.; Díaz-Somoano, M.; Martínez-Tarazona, M. R.; Maroto-Valer, M. M. Speciation of mercury in fly ashes by temperature programmed decomposition. *Fuel Process. Technol.* **2011**, *92* (3), 707–711.
- (46) Rumayor, M.; Lopez-Anton, M. A.; Díaz-Somoano, M.; Martínez-Tarazona, M. R. A new approach to mercury speciation in solids using a thermal desorption technique. *Fuel* **2015**, *160*, 525–530.
- (47) Zhao, H.; Yang, G.; Gao, X.; Pang, C. H.; Kingman, S. W.; Wu, T. Hg⁰ capture over CoMoS/γ-Al₂O₃ with MoS₂ nanosheets at low temperatures. *Environ. Sci. Technol.* **2016**, *50* (2), 1056–1064.
- (48) Li, G.; Shen, B.; Lu, F. The mechanism of sulfur component in pyrolyzed char from waste tire on the elemental mercury removal. *Chem. Eng. J.* **2015**, *273*, 446–454.